

NASA Technical Memorandum 104492
AIAA-91-1379

IN 20
47542
P. 18

Improved Thermodynamic Modeling of the No-Vent Fill Process and Correlation With Experimental Data

(NASA-TM-104492) IMPROVED THERMODYNAMIC
MODELING OF THE NO-VENT FILL PROCESS AND
CORRELATION WITH EXPERIMENTAL DATA (NASA)
18 p CSCL 21H

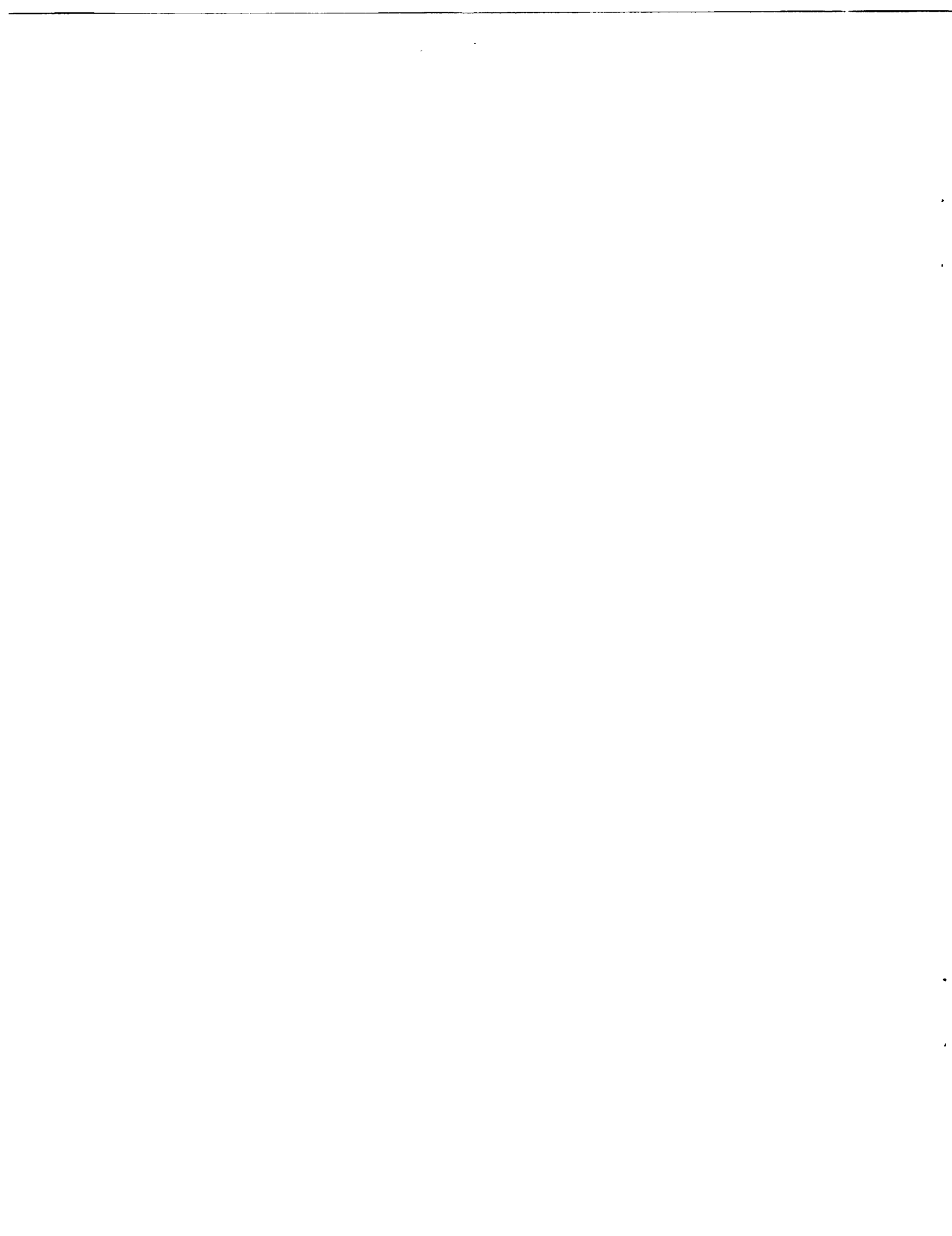
N92-11129

Unclas
63/20 0047542

William J. Taylor and David J. Chato
Lewis Research Center
Cleveland, Ohio

Prepared for the
26th Thermophysics Conference
sponsored by the American Institute of Aeronautics and Astronautics
Honolulu, Hawaii, June 24-26, 1991

NASA



IMPROVED THERMODYNAMIC MODELING OF THE NO-VENT FILL PROCESS
AND CORRELATION WITH EXPERIMENTAL DATA

W.J. Taylor* and D.J. Chato*
National Aeronautics and Space Administration
Lewis Research Center
Cleveland, Ohio 44135

Abstract

The United States' plans to establish a permanent manned presence in space and to explore the Solar System have created the need to efficiently handle large quantities of subcritical cryogenic fluids, particularly propellants such as liquid hydrogen and liquid oxygen, in low-to zero-gravity environments. One of the key technologies to be developed for fluid handling is the ability to transfer the cryogenes between storage and spacecraft tanks. The no-vent fill method has been identified as one way to perform this transfer. In order to understand how to apply this method, a model of the no-vent fill process is being developed and correlated with experimental data. The verified models then can be used to design and analyze configurations for tankage and subcritical fluid depots. This paper discusses the development of an improved macroscopic thermodynamic model of the no-vent fill process and correlates the analytical results from the computer program implementation of the model with experimental results for two different test tanks at NASA Lewis Research Center.

Nomenclature

A area
C_v specific heat constant volume
h specific enthalpy

\bar{h} Convection heat transfer coefficient
M mass
m mass flow rate
P pressure
Q heat input
q heat flux
T temperature
t time
U total internal energy
u specific internal energy
W work
 \dot{W} power

Greek Symbols:

ρ density
 λ spray cooling efficiency

Subscripts:

cond condensate
gas ullage gas
in inlet
inf interface
lg liquid/gas

*Aerospace Engineer, Member AIAA.

liq liquid
 par parasitic
 sat saturation
 sgas saturated gas
 tank tank
 wall tank wall

No-Vent Fill Process

The no-vent fill process was identified early on¹ as a key technology for the handling of cryogenic liquids in a low- to zero-gravity environment. The present procedure for the no-vent fill which incorporates tank chilldown via charge, hold, vent cycles was defined in Refs. 2 and 3. The no-vent fill process allows a propellant or storage tank to be filled or replenished without venting or requiring the tank contents to be positioned via a settling acceleration. Briefly the no-vent fill process proceeds as outlined below. The tank wall temperature, and thus the tank wall energy content, is reduced to an initial target value via a series of charge, hold, and vent cycles. The target temperature is selected to allow the transfer process to the tank to achieve 95 percent liquid fill by volume without exceeding a specified maximum pressure. Once the tank wall temperature has been reduced to the target temperature, the fill phase of the process can begin. During the fill phase, liquid is continuously injected into the tank until the desired fill level is achieved. Initially, vapor is generated as the incoming liquid cools the walls further. Liquid also begins to accumulate in the tank during this time. The accumulated bulk liquid compresses the vapor in the ullage space. Simultaneously, the vapor in the ullage is condensing due to heat and mass transfer to the incoming

liquid spray and the accumulating liquid. If the condensation of the ullage gas occurs at a sufficiently high rate, no ullage compression occurs; the pressure will, therefore, decrease after an initial pressure rise. Plots of the tank pressure versus time for two typical hydrogen no-vent fills from Ref. 6 are shown in Figs. 1 and 2. Figure 2 depicts a fill in which the tank pressure decreases after the initial pressure rise.

Macroscopic Thermodynamic Model

Chato⁴⁻⁶ has previously reported on the development of a macroscopic thermodynamic model for the no-vent fill process. This paper describes the latest revisions made in this model as it is implemented in the NVFILL program at NASA Lewis Research Center. Chato's original model divided the no-vent fill process into two steps. In the first step, the wall is chilled from its initial target temperature to the temperature of the incoming the liquid. In the second step, the bulk liquid accumulates and the ullage vapor is compressed and condensed. The key assumption made by Chato in analyzing the wall chilldown step of the no-vent fill process was that all of the incoming liquid was vaporized until the wall temperature matches the temperature of the incoming liquid. Based on this assumption and the first law of thermodynamics, the governing equations for the wall chilldown were as follows:⁴

$$-M_{\text{wall}} \frac{d(C_v T)}{dt} = \dot{m}_{\text{in}} (h_{\text{sgas}} - h_{\text{in}}) \quad (1)$$

$$\frac{dM_{\text{gas}}}{dt} = \dot{m}_{\text{in}} \quad (2)$$

$$M_{\text{gas}} \frac{du_{\text{gas}}}{dt} = \dot{m}_{\text{in}} (h_{\text{sgas}} - u_{\text{gas}}) \quad (3)$$

The basic equations presented by Chato⁴ for the liquid accumulation, vapor compression and condensation step are presented below:

$$\frac{dM_{gas}}{dt} = -\dot{m}_{cond} \quad (4)$$

$$\frac{d(M_{gas}u_{gas})}{dt} = \dot{m}_{cond}h_{gas} + \dot{W}_{lg} \quad (5)$$

$$\frac{dM_{liq}}{dt} = \dot{m}_{in} + \dot{m}_{cond} \quad (6)$$

$$M_{liq} \frac{du_{liq}}{dt} + u_{liq} \frac{dM_{liq}}{dt} + Q_{inf} + \dot{m}_{in}h_{in} + \dot{m}_{cond}h_{liq} = \dot{W}_{lg} \quad (7)$$

$$\frac{dM_{inf}}{dt} = 0 \quad (8)$$

$$Q_{inf} = \dot{m}_{cond}(h_{gas} - h_{liq}) \quad (9)$$

$$\dot{m}_{cond} = \frac{\bar{h}A_{inf}(T_{sat} - T_{liq})}{(h_{gas} - h_{liq})} \quad (10)$$

$$\dot{W}_{lg} = \frac{P_{gas}}{\rho_{liq}}(\dot{m}_{in} + \dot{m}_{cond}) \quad (11)$$

The convection heat transfer coefficient in Eq. (10) governs the heat transfer between the liquid spray droplets and the ullage vapor and is calculated from a correlation presented by Brown.⁷ The complete methodology employed in using this correlation is presented in Ref. 5.

Comparisons of the results from this model with test data, presented in Ref. 6, indicated the need to change the model for modeling the top spray fill configurations tested at NASA Lewis in the Cryogenic Components Laboratory Site 7 (CCL-7) test rig. The basic modifications allowed for the accumulation of liquid before

the wall is completely cooled and for the parasitic heating of the accumulated bulk liquid, as initially these were thought to be largest sources of error in the model. The parasitic heating of the bulk liquid is defined as the heat leaks to the liquid in the tank due to either the experimental setup or the ambient environment. In the CCL-7 test rig, as described in Ref. 9, these heat leaks are exemplified by the axial conduction of heat along the tank walls from the top lid mounting flange and the heat radiated from the outer wall of the vacuum jacket to the inner wall where the heat is conducted into the bulk fluid. These modifications to the model required Eq. (1) to be changed as follows:

$$-M_{wall} \frac{d(c_v T)}{dt} = \lambda \dot{m}_{in}(h_{sgas} - h_{in}) \quad (12)$$

where λ is the spray cooling efficiency. The spray cooling efficiency is defined as the fraction of the incoming liquid mass that is vaporized through contact with the tank walls during any time increment. Thus, the value of the spray cooling efficiency is between 0 and 1. The partial vaporization of the incoming fluid necessitated the development of a new equation for the liquid mass accumulation to replace Eq. (6).

$$\frac{dM_{liq}}{dt} = (1 - \lambda)\dot{m}_{in} + \dot{m}_{cond} \quad (13)$$

Additionally, Eq. (14) replaced Eqs. (2) and (4) in the original model, with λ going to 0.0 when the wall has been chilled to the incoming liquid temperature.

$$\frac{dM_{gas}}{dt} = \lambda \dot{m}_{in} - \dot{m}_{cond} \quad (14)$$

Equation (7) was modified to account for the parasitic heating of the accumulated bulk liquid resulted as shown below:

$$M_{11q} \frac{du_{11q}}{dt} + u_{11q} \frac{dM_{11q}}{dt} + Q_{inf} \quad (15)$$

$$+ Q_{par} + \dot{m}_{in} h_{in} + \dot{m}_{cond} h_{11q} = \dot{W}_{1g}$$

Equation 5, which performs the energy balance for the ullage vapor, was modified to the form shown in Eq. (16).

$$\frac{dM_{gas} U_{gas}}{dt} = u_{gas} \frac{dM_{gas}}{dt} - \dot{m}_{cond} h_{gas} \quad (16)$$

$$+ \dot{W}_{1g} + \lambda \dot{m}_{in} (h_{sgas} - u_{gas})$$

Equation (11) was also revised to account for the partial vaporization of the incoming fluid.

$$\dot{W}_{1g} = \frac{P_{gas}}{\rho_{11q}} ((1-\lambda)\dot{m}_{in} + \dot{m}_{cond}) \quad (17)$$

Once this basic model encompassing Eqs. (8) to (10) and (12) to (17) was developed, it was implemented in the NVFILL computer program.

NVFILL Computer Program

The NVFILL program was written by Chato to implement the macroscopic thermodynamic model. It uses an explicit time-marching solution of the basic thermodynamic equations presented in the previous section. Both the original and the revised implementations of the model in the NVFILL program assume that all of the heat and mass transfer at the liquid vapor interface occurs between the ullage vapor and the incoming liquid spray droplets. The heat and mass transfer that occurs at the free surface of the accumulated bulk liquid is not considered. The original version of the code followed the two-step procedure delineated in the previous section. During the first step of the fill process, Eqs. (1) to (3) are solved for each time increment. Upon the completion of the first

step, the remaining equations, Eqs. (4) to (11), are solved for each time increment during the second step of the process.

The logic flow of the program had to be modified to account for the partial vaporization of the incoming liquid. Rather than having a two step procedure with the sequential performance of the two steps, now the wall chilldown and the liquid accumulation calculations, Eqs. (8) to (10) and Eqs. (12) to (17), are performed in each time step until the wall is chilled down. Once the wall chilldown is complete, only Eqs. (8) to (10) and (13) to (17), with λ equal to 0, are evaluated in each time step. The thermodynamic properties of the fluid are evaluated as required in each time step via calls to the GASP program.⁸ The latest version of the NVFILL program (5.4) is written in Fortran and runs on IBM PC compatible microcomputers.

Empirical Data

Receiver Tank Configuration

In the CCL-7 test rig, which is described in detail in Ref. 9, the liquid is thermally conditioned in the supply tank prior to performing the transfer. Two different size receiver tanks are used. The tank volumes are 1.24 ft³ for the small receiver tank and 5.0 ft³ for the large receiver tank. Both tanks have cylindrical body sections with an elliptical bottom dome and a lid. Figure 3 is a schematic of the tank geometries. Both receiver tanks have a conical spray nozzle mounted in the top dome which sprays downward. The spray half angle is 60°. The tanks are both commercial vacuum jacketed dewars constructed of 304 stainless steel.

CCL-7 Large Receiver Tank

The results from the initial series of tests, during which 9 no-vent fill tests were performed, are presented in Ref. 6. This testing demonstrated the feasibility of the no-vent fill process with both liquid hydrogen and liquid nitrogen. The graphs of the tank pressure histories for 4 of these tests along with the original and revised analytical modeling results are presented in Figs. 4 to 7. All of the test parameters and conditions are presented in detail in Ref. 6.

This initial testing was conducted to verify the operation of the facility and the data collection system. More rigorous experimentation with this tank is currently being conducted.

CCL-7 Small Receiver Tank

A series of 18 liquid hydrogen no-vent fill tests with a top spray fill configuration were performed using the 1.24 ft³ dewar. The primary variables in this test series were the liquid inlet mass flow rate, which ranged from 0.3 to 3.8 lb_m/min, and the initial tank wall temperature, which ranged from 55.3 to 167 °R. The liquid inlet temperatures ranged from 32.8 to 35.9 °R. While not all of the tests were successful in achieving the target fill level of 95 percent, half of the tests were completed with final fill levels at or above 94 percent. However, neither of the two tests conducted at the low inlet mass flow rates (approximately 0.3 lb_m/min) were successful, and only three of the eight tests with inlet mass flow rates of approximately 0.7 lb_m/min were successful. Table 1 presents a summary of the test parameters for each run. A more complete discussion of all the tests and the results obtained can be found in Ref. 10.

Analytical Results

CCL-7 Large Receiver Tank

The results of the nine large receiver tank tests were analyzed using the revised version of the NVFILL program. The results for 4 of these analyses (2 nitrogen cases and 2 hydrogen cases) are presented in Figs. 4 to 7. Only 4 cases were selected for presentation in this paper, as they represent the most significant results obtained with the revised model. Both of the nitrogen test cases,⁶ N2 and N3, (Figs. 4 and 5) exhibit a large initial pressure rise followed by a pressure decay over the remaining duration of the test. The two hydrogen cases presented, H2 and H4, (Figs. 6 and 7) were the only successful tests with hydrogen in the initial testing at CCL-7. The remaining test cases were of such short duration, they were not included here. The model results of Ref. 6 are included in Figs. 4 to 7 for comparison purposes. These new analyses also provided the opportunity to reexamine the experimental results and, based on this examination, revise two of the analysis input parameters.

The initial average tank wall temperature had to be changed in most of the analyses. The original model inputs for the tank wall temperature were based on a simple volume weighted arithmetic average of the tank wall temperatures. These average wall temperatures were calculated from a discrete nodalization of the tank walls which was based on the location of temperature sensors mounted to the wall. The revised temperature calculations use the same nodalization but also account for the temperature dependency of the specific heat of the wall material. This approach was necessitated by the presence of large temperature gradients axially along the tank wall at the start of the tests and the large

variation in the specific heat of stainless steel over the observed temperatures. The resulting initial average wall temperatures are higher than those calculated assuming a constant specific heat for the tank wall and provide a better estimate of the initial tank wall energy content.

The liquid inlet temperature was the other parameter to be revised. Based on the temperature difference measured between the supply tank fluid and the liquid temperature measured at the flow meter, a distance of approximately 20 ft, the liquid inlet temperatures for some of the hydrogen tests were increased approximately 1 to 2 °R. These temperature increases account for the heat leaks to the incoming liquid hydrogen due to the distance (approximately 15 ft) from the liquid temperature sensor to the tank inlet. The temperature difference between the supply tank and the flow meter was inversely proportional to the liquid mass flow rate, thus for the high flow rate cases the temperature difference became negligible. The nitrogen test cases were not affected as the liquid mass flow rates are 3 to 10 times higher than those used in the hydrogen test cases. The input parameters for the two sets of analyses are compared in Table 2.

One other parameter to be considered in these analyses is the tank-mass-to-volume ratio. The results presented in Ref. 6, used a reduced tank-mass-to-volume ratio of 2.1 lb_m/ft. This effectively reduced the energy content of the tank wall at the start of the fill process. As discussed in Ref. 6, this is an attempt to compensate for the fact that the tank lid assembly does not cool down significantly during the fill tests conducted with high inlet mass flow rates, thus the energy in the lid is not transferred to the fluid in the tank. The revised analyses also used this reduced value.

The revised version of the NVFILL program requires two additional inputs, one for the parasitic heat leak and the second for the spray cooling efficiency. All of the analytical results presented in this paper used a value of 0.00 for the parasitic heating due to the small magnitude of the heat leak and the short duration of the tests. Boiloff tests conducted at CCL-7 with the two receiver tanks, filled to various levels with H₂, indicated the parasitic heat leaks to the tank contents are on the order of 18 Btu/hr and 30 Btu/hr for the small and large receiver tanks respectively. With test durations ranging from approximately 1.5 to 7.0 min for the small receiver tank, the total parasitic heat leak to the tank has a maximum value of 2.1 Btu. Similarly the total parasitic heat leak for the large receiver tank tests is approximately 7.5 Btu. These small heat leaks are negligible in comparison with the energy of the incoming liquid, and thus do not impact the final pressure in the receiver tank.

Analysis of the tank and spray nozzle geometry determined that the maximum percentage of the incoming spray that could strike the tank sidewalls was 63 percent after liquid accumulated in the elliptical bottom dome section of the receiver tanks. Assuming a constant inlet mass flow rate, the percentage of the incoming flow that strikes the sidewalls decreases to 0 percent over the duration of the fill. Thus the time-averaged value is 32 percent. Based on the information in Ref. 11, the spray cooling efficiency for droplet sprays varies between 3 and 20 percent. Multiplying these efficiencies by the percentage of the incoming liquid spray mass that strikes the side walls, yields an overall average spray cooling efficiency that ranges between 0.1 and 6.4 percent for our test configurations. A value (5 percent) near the top of this range was

selected for the analyses presented in this paper, as the wall chilldown was accomplished fairly rapidly during the tests. The model implementation assumes the spray cooling efficiency remains constant until the wall chilldown is complete. In reality, the spray cooling efficiency will increase as the wall is chilled and the temperature difference between the wall and the liquid spray droplet is reduced.

The plots of the data and the analysis results for the two nitrogen cases are presented in Figs. 4 and 5. The partial evaporation of the incoming spray provides a much more accurate representation of the initial pressure spike for the hot wall cases when compared with the analytical results presented in Ref. 6; however, analysis of the bulk liquid accumulation, vapor compression and condensation step still shows a discrepancy between the experimental and the analytical results. This difference can be attributed to the model implementation, which forces the tank's contents to thermodynamic equilibrium instantaneously when the conditions in the tank are such that bulk boiling occurs in the accumulated liquid.

The five hydrogen test cases discussed in Ref. 6 were also analyzed. The empirical data and the results from the modified NVFILL program for two of these tests are presented in Figs. 6 and 7. The analytical results for these cases were affected most by the changes in the input parameters for the initial wall temperatures and the liquid inlet temperature. These changes produced better correlation between the analytical and the test results, especially with regard to the magnitude of the initial pressure rise for the H4 case and the final tank pressure for the H2 case. The correlation between the test data and the analysis results for the different tests was improved in all cases.

CCL-7 Small Receiver Tank

All 18 of the hydrogen top spray configuration no-vent fill tests conducted at CCL-7 using the small receiver tank were analyzed with the revised NVFILL program. As was the case for the large receiver tank tests, the liquid inlet temperatures for the analyses were estimated based on the temperature difference of the fluid measured between the supply tank and the flowmeter. The inlet mass flow rates for these tests had to be calculated from the tank fill level versus time data due to a failure in the instrumentation associated with the flowmeter. Table 3 summarizes the variable input parameters for each case.

The tank-mass-to-volume ratio used in all these analyses was $6.96 \text{ lb}_m/\text{ft}^3$. The analytical results for the 15 of the 18 test cases along with the empirical data are presented in Figs. 8 to 22. The results for the tests identified as 9088A, 9088E and 9094H were not included due to anomalies present in the data. Each of the figures depicts the tank pressure versus time for the respective test run. The results for the low flow rate ($0.3 \text{ lb}_m/\text{min}$) cases (9072A and 9075A) are shown in Figs. 8 and 9. The empirical data clearly indicate that there is some error in the test instrumentation particularly with regard to the liquid level in the tank at the initiation of the test and the liquid inflow rate. Despite these errors, the program results track the pressure history of the tank with a maximum difference from the experimental data of 5 psia. It also appears that the program slightly over predicts the tank pressure at a given fill level.

The six moderate flow rate (0.6 to $0.8 \text{ lb}_m/\text{min}$) cases (9072B, 9075B, 9075D, 9080A, 9081A, and 9081E) were also analyzed. As shown in Figs. 10 to 15, excellent results were obtained for all of the cases, the

predicted pressures differing from the empirical data by less than 3 psia. The results show the importance of the liquid inlet temperature in the analysis as the incoming liquid energy dominates the final condition of the fluid in the tank. Therefore, in order to obtain the analytical results shown in Figs. 10 to 15, the inlet temperatures were adjusted upward by approximately 1 °R, again accounting for heat leaks to the incoming liquid. With regard to the initial pressure rise, the initial temperature of the tank wall and the spray cooling efficiency strongly influence the analytical results, particularly for low inlet mass flow rates.

In the 8 high inlet flow rate cases (9093A, 9093B, 9093C, 9093D, 9094A, 9094B, 9094C, and 9094H), the liquid inlet mass flow rates ranged from 2.0 to 3.8 lb_m/min. Initial analyses, not presented herein, of all but two of these test cases did not correlate well with the experimental data. The analytical results exhibited an initial pressure spike of shorter duration and larger magnitude than the test data. Examination of the test data showed that the lid assembly was not being cooled during the fill process. This phenomenon was also observed in the large receiver tank⁶ tests. Instead of reducing the tank mass-to-volume ratio, as was done previously, new estimates of the tank wall temperature were made by accounting for the temperature change undergone by the lid and thereby the energy removed. As can be seen in Figs. 16 and 18 to 21, these reduced initial wall temperatures enabled the model to replicate the experimental data quite well. For the two cases, 9093B and 9094C which are plotted in Figs. 17 and 22, where the model did predict the behavior of the receiver tank without having to reducing the average initial wall temperature, an examination of the test data revealed

the lid assembly was cooled down at the beginning of the test and thus had little influence on the tank wall energy content and thereby the energy to be transferred to the incoming liquid. The major differences between the test data and the analytical results for the high flow rate cases are in the predicted initial pressure rise rates; indicating that either the initial wall temperatures and/or the specified spray cooling efficiency used in the analytical model were too high.

Summary

A simple macroscopic thermodynamic model of the no-vent fill process developed by Chato was revised to account for the partial vaporization of the incoming liquid spray and for the parasitic heat leak to the accumulated bulk liquid. This revised model was implemented in a new version of the NVFILL computer program and the results were compared with empirical data for two receiver tanks tested at NASA Lewis. The modifications improved the correlation between analytical and experimental results for both hydrogen and nitrogen. However, based on the results of multiple runs of the model, the largest improvements in the analytical results were due to the more exact calculation of the initial wall temperatures and increasing the incoming liquid temperature to account for the parasitic heat leaks to the liquid in the lines between the flowmeter and the receiver tank. The analytical results obtained with the revised inputs, in conjunction with the revised model correlate with both the process time line and the tank pressure versus the volumetric liquid fill percentage. With sufficient attention to the process inputs, results were obtained that differ by less than 5 psia from the experimental data.

Future efforts will continue to seek to improve the model and validate the results against data from other no-vent fill tests being performed; the final step in the development of this design tool will have to wait until the model can be validated against test data for tanks in a low-gravity environment.

References

1. Morgan, L.L, et al., "Orbital Tanker Design Data Study," Lockheed Missiles and Space Company, LMSC-A748410, 1965.
2. Merino, F., et al., "Filling of Orbital Fluid Management Systems," NASA CR-159404, July 1978.
3. Merino, F., J.A. Risberg and M.Hill, "Orbital Refill of Propulsion Vehicle Tankage," NASA C-159722, February 1980.
4. Chato, D.J., "Thermodynamic Modelling of the No-Vent Fill Methodology for Transferring Cryogenics in Low Gravity," AIAA Paper 88-3403, July 1988.
5. Chato, D.J., "Analysis of the Nonvented Fill of a 4.95-Cubic-Meter Lightweight Liquid Hydrogen Tank," NASA TM-102039, August 1989.
6. Chato, D.J., M. Moran, and T. Nyland, "Initial Experimentation on the Nonvented Fill of a 0.14 m³ (5 ft³) Dewar with Nitrogen and Hydrogen," AIAA Paper 90-1681, June 1990.
7. Brown, G., "Heat Transfer by Spray Cooling," General Discussion on Heat Transfer, IME and ASME, London, September 1951, pp. 49-52.
8. Hendricks, R.C., A.K. Baron and I.C. Peller, "GASP - A Computer Code for Calculating the Thermodynamic and Transport Properties for Ten Fluids: Parahydrogen, Helium, Neon, Methane, Nitrogen, Carbon Monoxide, Oxygen, Fluorine, Argon, and Carbon Dioxide," NASA Technical Note NASA TN D-7808, February 1975.
9. Moran, M.E., T.W. Nyland, and S.S. Papell, "Liquid Transfer Cryogenic Test Facility - Initial Hydrogen and Nitrogen No-Vent Fill Data," NASA TM-102572, March 1990.
10. Moran, M.E., T.W. Nyland, and S.L. Driscoll, "Hydrogen No-Vent Fill Testing in a 34 l (1.2 ft³) Tank," Cryogenic Engineering Conference, June 1991.
11. Hewitt, G. F., Multiphase Science and Technology, Volume 1, Chapter 1, Hemisphere Publishing, New York, 1982.

TABLE 1. - CCL-7 SMALL RECEIVER TANK TEST PARAMETERS

Test run, ID	Liquid inlet temperature, °R	Initial average wall temperature, °R	Liquid inlet mass flow rate, lb/min	Initial tank pressure, psia	Final fill, percent
9072A	36.4	114	0.3	3.0	8
9072B	34.3	83	.7	3.2	98
9075A	39.2	132	.3	2.9	10
9075B	37.4	81	.6	3.1	10
9075D	34.7	100	.6	3.1	67
9080A	34.9	56	.7	4.6	98
9081A	37.6	64	.6	3.6	50
9081E	34.1	79	.6	3.9	96
9088A	37.1	80	.6	3.8	54
9088E	34.9	74	.8	3.8	99
9093A	33.7	128	2.0	3.9	98
9093B	33.7	84	2.8	3.6	99
9093C	33.6	107	3.3	3.6	97
9093D	33.2	99	3.8	4.0	99
9094A	35.9	113	3.6	3.9	95
9094B	35.9	103	3.0	3.5	90
9094C	35.7	98	2.3	3.9	91
9094H	32.8	86	3.8	5.4	96

TABLE 2. - CCL-7 LARGE RECEIVER TANK ANALYSIS INPUT PARAMETER COMPARISON

Test run, ID	Original inlet temperature, °R	Original initial wall temperature, °R	Revised inlet temperature, °R	Revised initial wall temperature, °R
H2	34	103	35.5	153
H4	34	55	34.5	109
N2	126	273	126	315
N3	122	299	122	333

TABLE 3. - CCL-7 SMALL RECEIVER TANK ANALYSIS INPUT PARAMETERS

Test run, ID	Inlet mass flow rate, lb _m /min	Inlet temperature, °R	Initial wall temperature, °R	Initial tank pressure, psia
9072A	0.3	42.0	128.4	3.0
9072B	.7	35.5	96.5	3.2
9075A	.3	43.0	146.6	2.9
9075B	.6	38.0	91.3	3.1
9075D	.6	36.0	109.3	3.1
9080A	.7	35.7	55.3	4.6
9081A	.6	38.2	72.9	3.6
9081E	.6	35.5	78.9	3.9
9093A	2.0	33.7	96.0	3.9
9093B	2.8	33.7	104.0	3.6
9093C	3.3	33.6	100.0	3.6
9093D	3.8	33.2	90.0	4.0
9094A	3.6	35.9	75.0	3.9
9094B	3.0	35.9	53.0	3.5
9094C	2.3	35.7	100.0	3.9

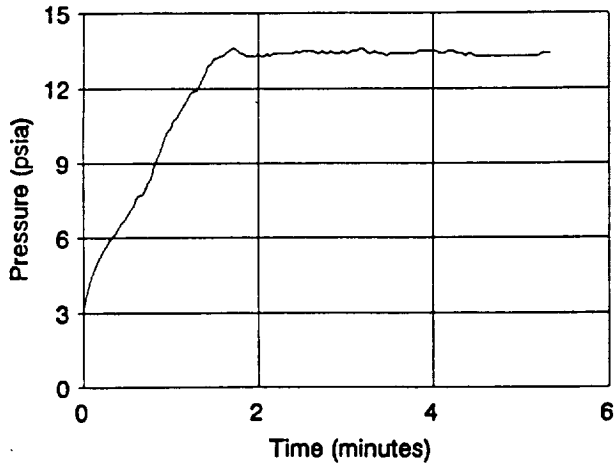


Figure 1: Typical Hydrogen No-Vent Fill Pressure History

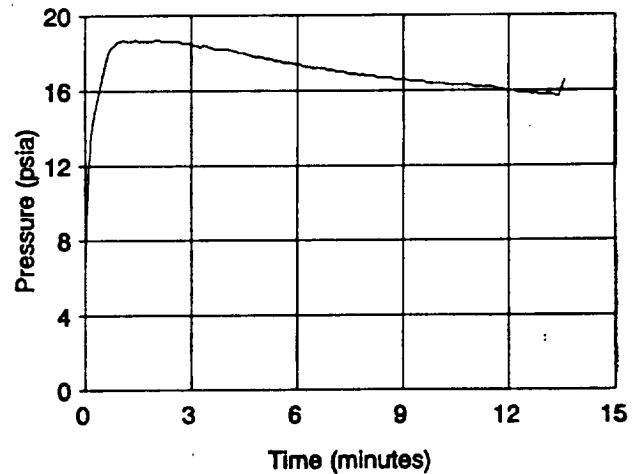


Figure 2: No-Vent Fill Pressure History with Pressure Decrease During Fill Process

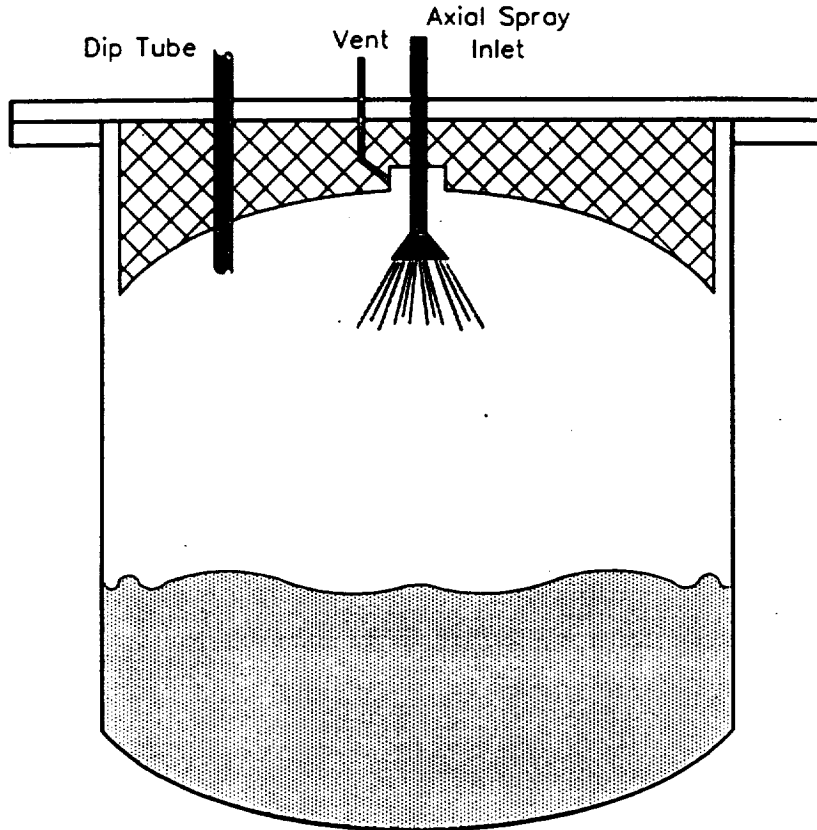


Figure 3: CCL-7 Top Spray Test Tank Geometry Schematic

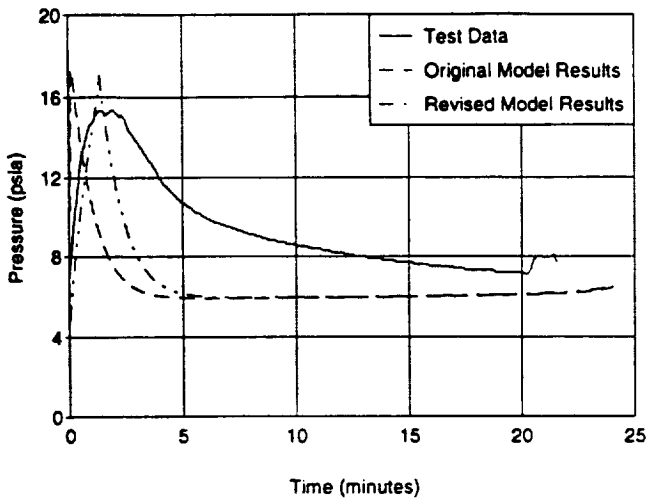


Figure 4: Pressure History Comparison for Test N2

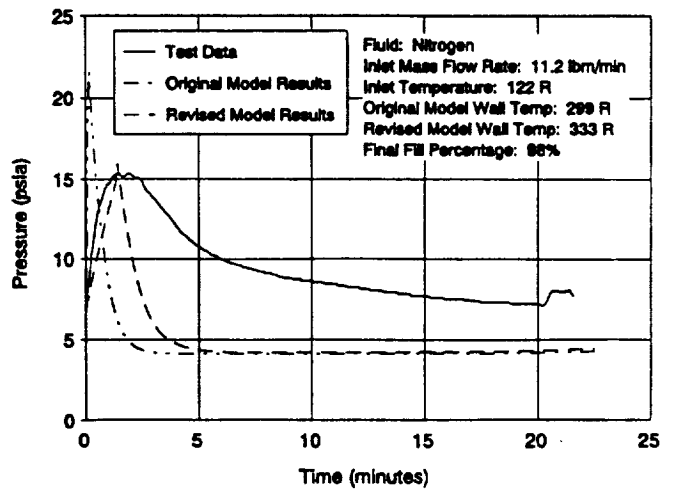


Figure 5: Pressure History Comparison for Test N3

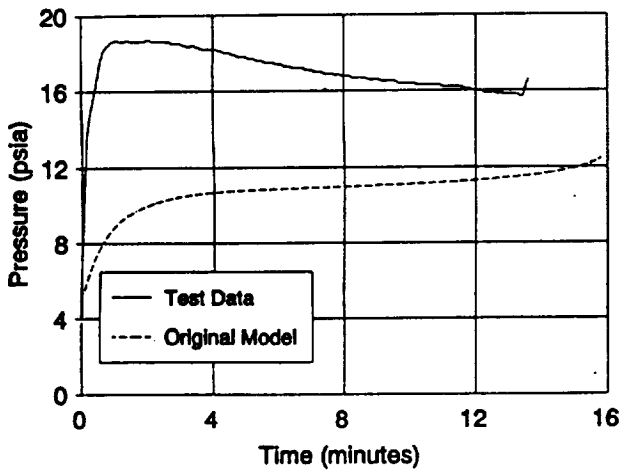


Figure 6a: Original Model Pressure History Comparison with Test Data for Test H2

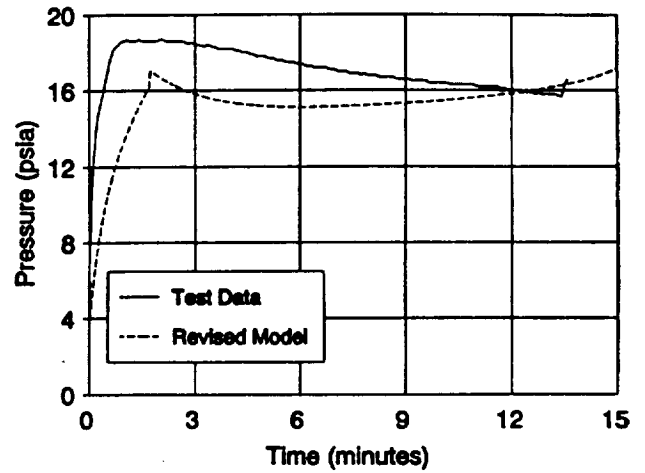


Figure 6b: Revised Model Pressure History Comparison with Test Data for Test H2

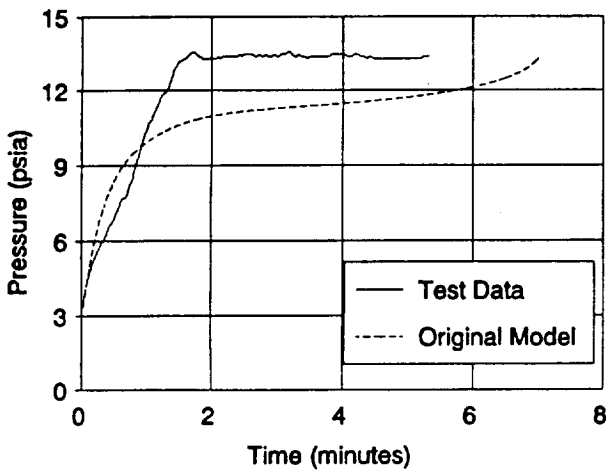


Figure 7a: Original Model Pressure History Comparison with Test Data for Test H4

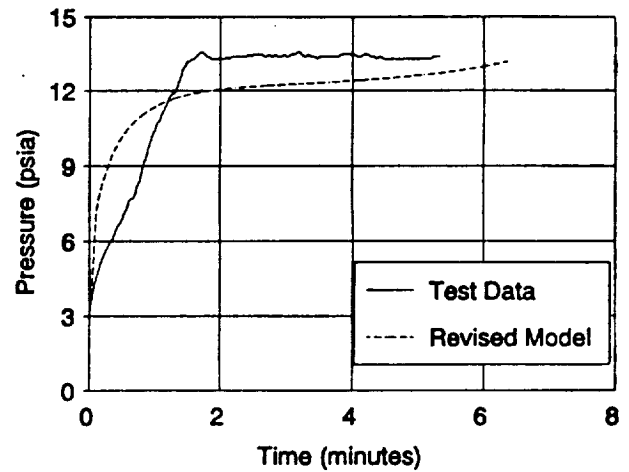


Figure 7b: Revised Model Pressure History Comparison with Test Data for Test H4

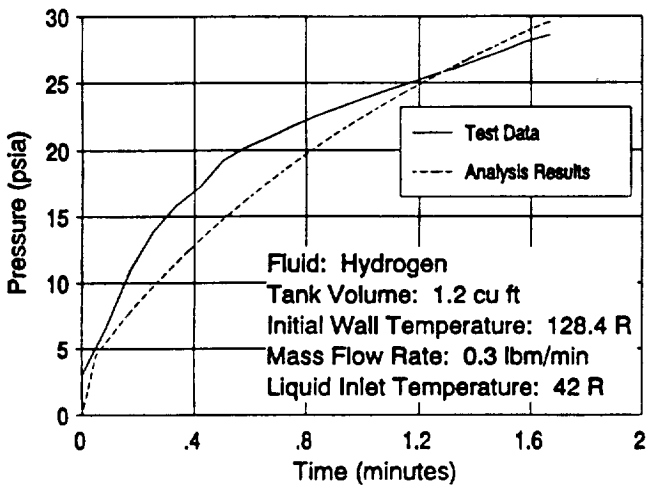


Figure 8: Pressure History for No-Vent Fill Test 9072A

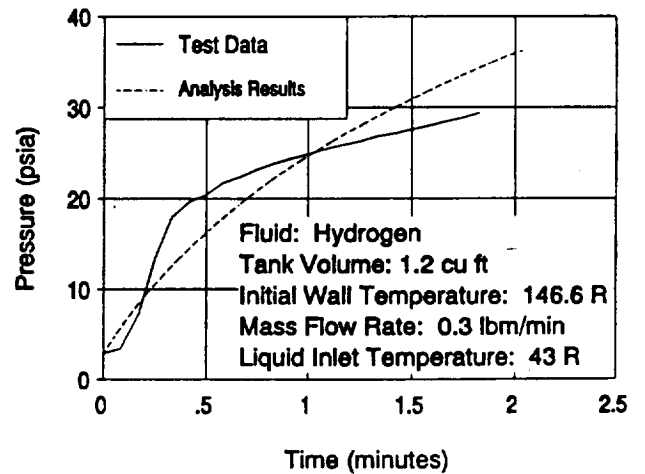


Figure 9: Pressure History for No-Vent Fill Test 9075A

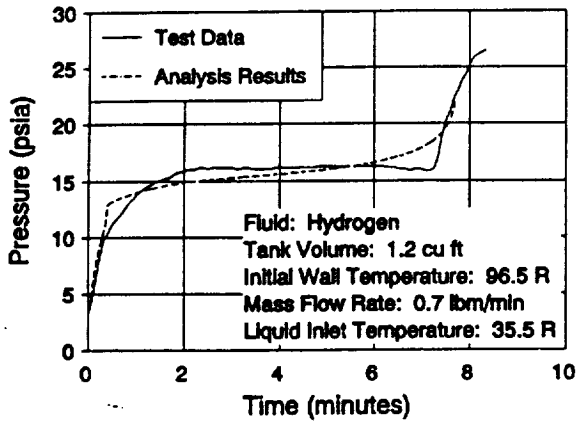


Figure 10: Pressure History for No-Vent Fill Test 9072B

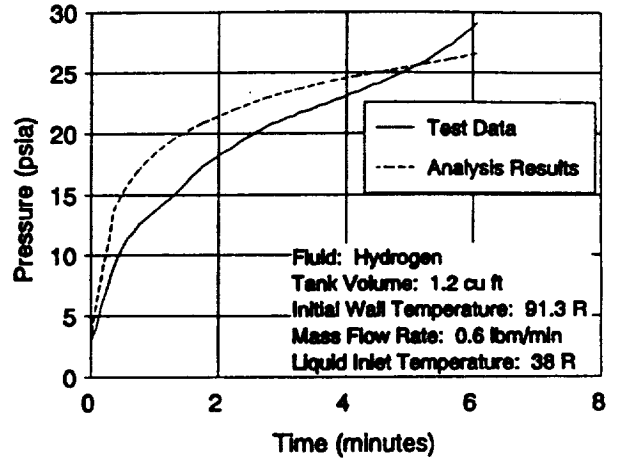


Figure 11: Pressure History for No-Vent Fill Test 9075B

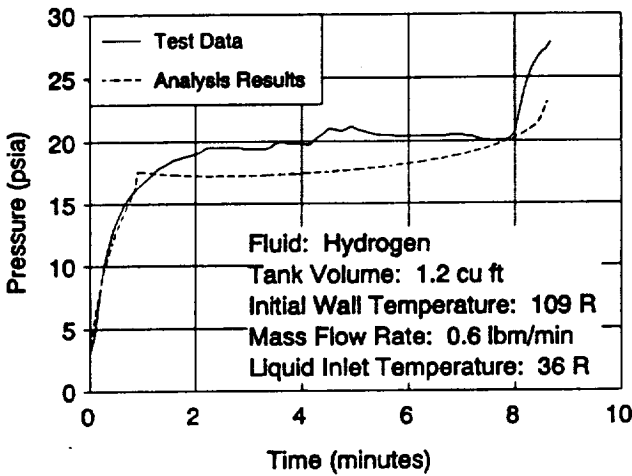


Figure 12: Pressure History for No-Vent Fill Test 9075D

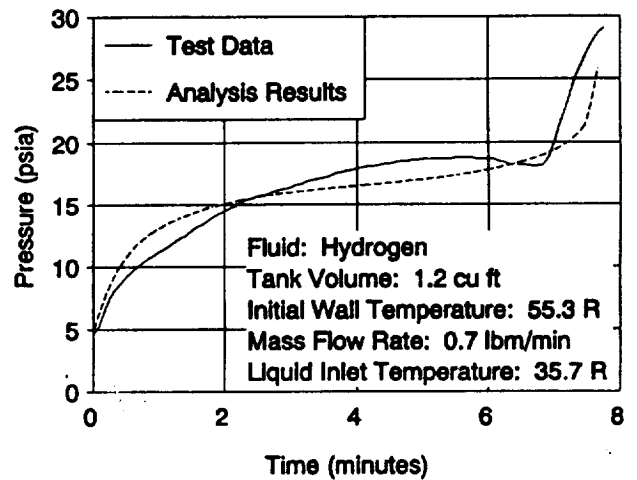


Figure 13: Pressure History for No-Vent Fill Test 9080A

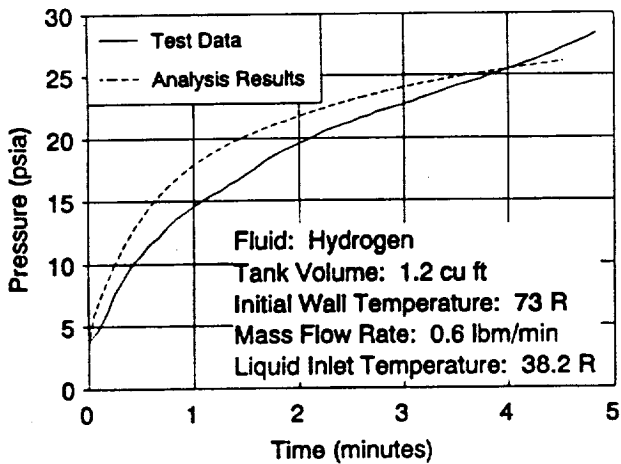


Figure 14: Pressure History for No-Vent Fill Test 9081A

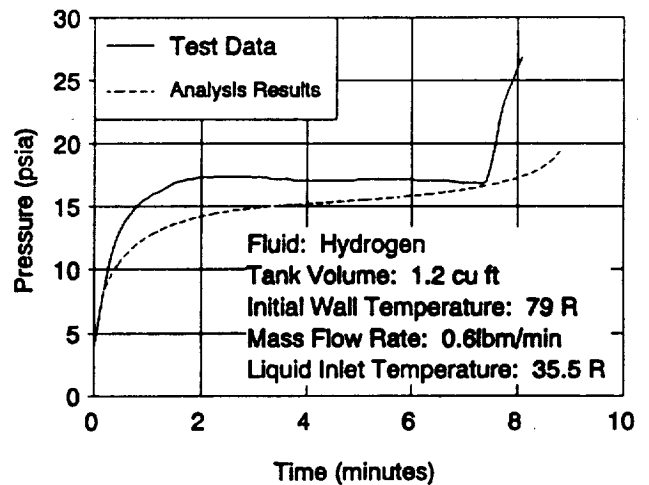


Figure 15: Pressure History for No-Vent Fill Test 9081E

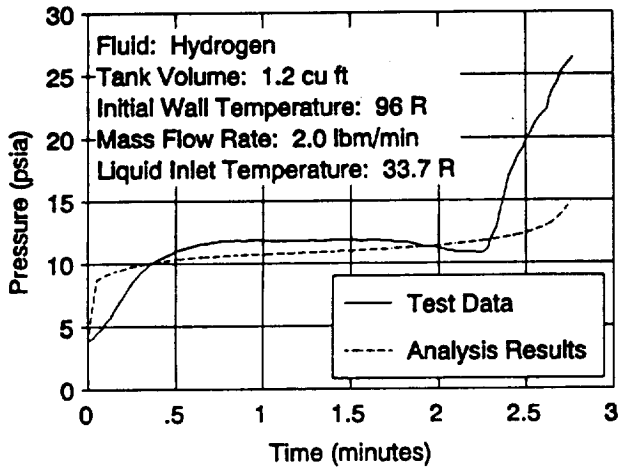


Figure 16: Pressure History for No-Vent Fill Test 9093A

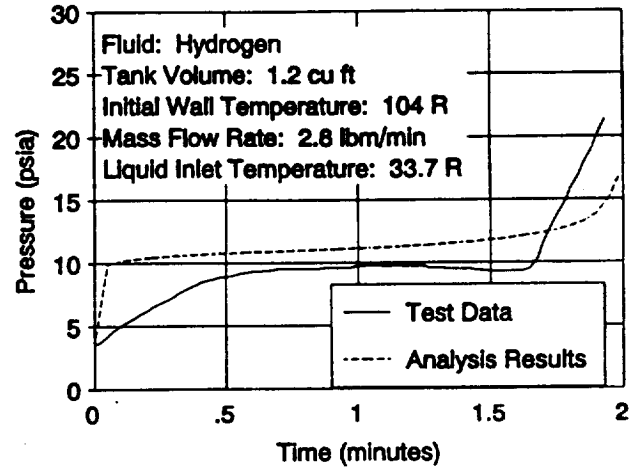


Figure 17: Pressure History for No-Vent Fill Test 9093B

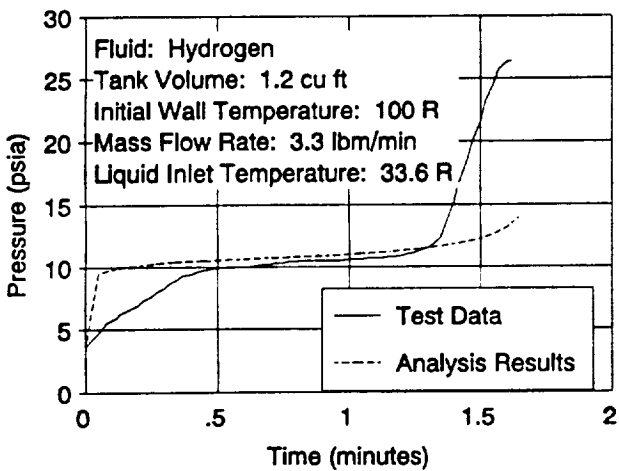


Figure 18: Pressure History for No-Vent Fill Test 9093C

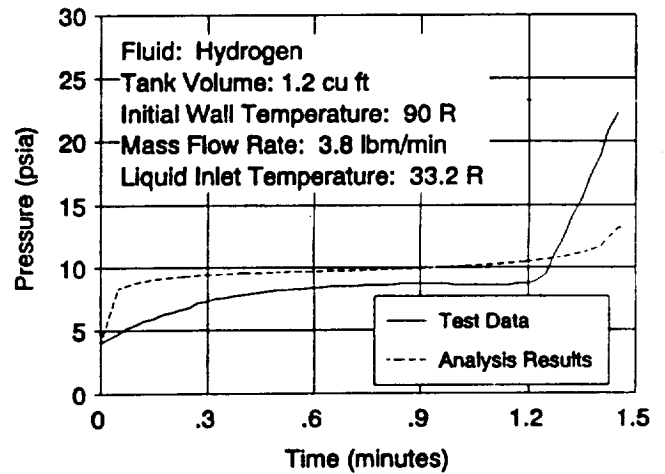


Figure 19: Pressure History for No-Vent Fill Test 9093D

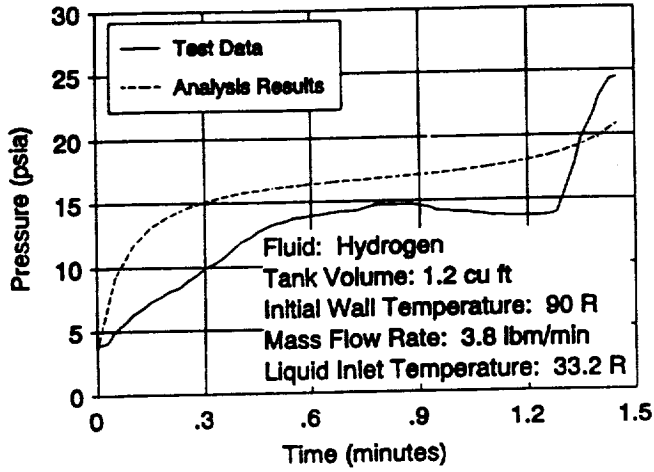


Figure 20: Pressure History for No-Vent Fill Test 9094A

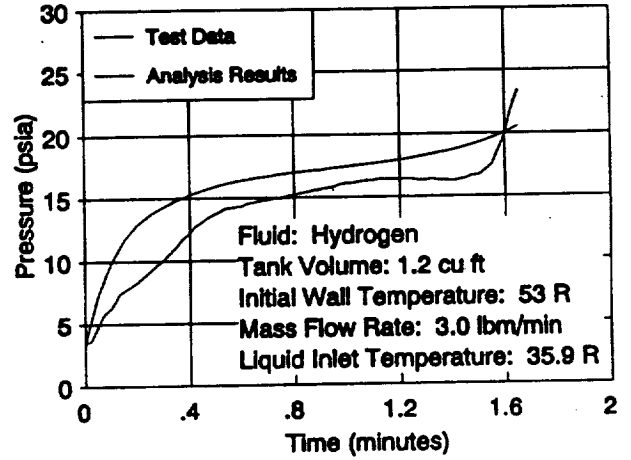


Figure 21: Pressure History for No-Vent Fill Test 9094B

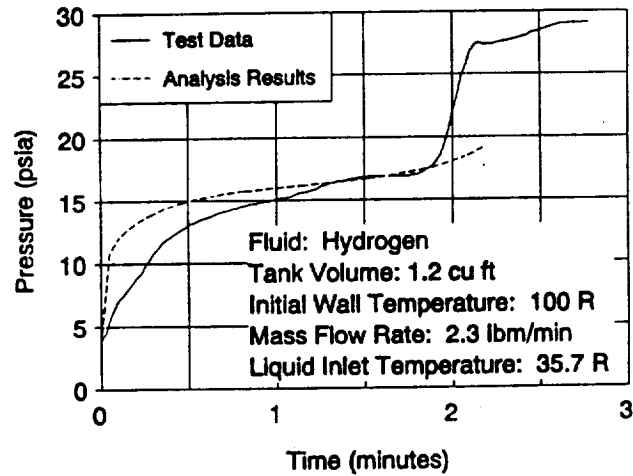


Figure 22: Pressure History for No-Vent Fill Test 9094C

1. Report No. NASA TM-104492 AIAA-91-1379		2. Government Accession No.		3. Recipient's Catalog No.	
4. Title and Subtitle Improved Thermodynamic Modeling of the No-Vent Fill Process and Correlation With Experimental Data				5. Report Date	
				6. Performing Organization Code	
7. Author(s) William J. Taylor and David J. Chato				8. Performing Organization Report No. E-6350	
				10. Work Unit No. 506-48	
9. Performing Organization Name and Address National Aeronautics and Space Administration Lewis Research Center Cleveland, Ohio 44135-3191				11. Contract or Grant No.	
				13. Type of Report and Period Covered Technical Memorandum	
12. Sponsoring Agency Name and Address National Aeronautics and Space Administration Washington, D.C. 20546-0001				14. Sponsoring Agency Code	
15. Supplementary Notes Prepared for the 26th Thermophysics Conference sponsored by the American Institute of Aeronautics and Astronautics, Honolulu, Hawaii, June 24-26, 1991. Responsible person, William J. Taylor (216) 433-2845.					
16. Abstract The United States' plans to establish a permanent manned presence in space and to explore the Solar System have created the need to efficiently handle large quantities of subcritical cryogenic fluids, particularly propellants such as liquid hydrogen and liquid oxygen, in low- to zero-gravity environments. One of the key technologies to be developed for fluid handling is the ability to transfer the cryogenics between storage and spacecraft tanks. The no-vent fill method has been identified as one way to perform this transfer. In order to understand how to apply this method, a model of the no-vent fill process is being developed and correlated with experimental data. The verified models then can be used to design and analyze configurations for tankage and subcritical fluid depots. This paper discusses the development of an improved macroscopic thermodynamic model of the no-vent fill process and correlates the analytical results from the computer program implementation of the model with experimental results for two different test tanks at NASA Lewis Research Center.					
17. Key Words (Suggested by Author(s)) Propellant transfer Reduced gravity Space technology experiment			18. Distribution Statement Unclassified - Unlimited Subject Category 20		
19. Security Classif. (of the report) Unclassified		20. Security Classif. (of this page) Unclassified		21. No. of pages 18	22. Price* A03

